CrossMark

PEER REVIEWED

Thermal Conductivity in Suspension Sprayed Thermal Barrier Coatings: Modeling and Experiments

Ashish Ganvir[1] · Chamara Kumara[1] · Mohit Gupta[1] · Per Nylen[1]

Abstract Axial suspension plasma spraying (ASPS) can generate microstructures with higher porosity and pores in the size range from submicron to nanometer. ASPS thermal barrier coatings (TBC) have already shown a great potential to produce low thermal conductivity coatings for gas turbine applications. It is important to understand the fundamental relationships between microstructural defects in ASPS coatings such as crystallite boundaries, porosity etc. and thermal conductivity. Object-oriented finite element (OOF) analysis has been shown as an effective tool for evaluating thermal conductivity of conventional TBCs as this method is capable of incorporating the inherent microstructure in the model. The objective of this work was to analyze the thermal conductivity of ASPS TBCs using experimental techniques and also to evaluate a procedure where OOF can be used to predict and analyze the thermal conductivity for these coatings. Verification of the model was done by comparing modeling results with the experimental thermal conductivity. The results showed that the varied scaled porosity has a significant influence on the thermal conductivity. Smaller crystallites and higher overall porosity content resulted in lower thermal conductivity. It was shown that OOF could be a powerful tool to predict and rank thermal conductivity of ASPS TBCs.

Keywords finite element modeling · microstructure · OOF2 · suspension plasma spraying · thermal barrier coatings · thermal conductivity

Introduction

Columnar structured thermal barrier coatings (TBCs) are of great interest in the gas turbine industry due to their better strain tolerance ability than conventional TBCs (Ref 1-3). Conventionally, these columnar structured TBCs were produced for several years by electron beam vapor deposition technique (EBPVD) (Ref 4). Suspension plasma spraying (SPS), which is much cheaper and faster technique than EBPVD, has also shown a great potential in recent years to produce similar type of columnar structured TBCs (Ref 3, 5-7).

It has been a great challenge for researchers to obtain low thermal conductivity columnar structured TBCs using either of the above-mentioned techniques (Ref 2, 3, 7-11). In recent work done by the authors, an axial suspension plasma spraying (ASPS) has been shown to be a promising and advanced thermal spray technique to produce both columnar structured as well as low thermal conductivity TBCs (Ref 12-14).

SPS coatings have been shown to consist of a microstructure with several features such as very fine crystallites, submicron or nano-sized pores, segmented cracks or inter-columnar spacing, inter-pass porosity bands etc. (Ref 5, 7, 12, 13). These varied features make the SPS coating microstructure very distinct than the conventional

✉ Mohit Gupta
mohit-kumar.gupta@hv.se

Ashish Ganvir
ashish.ganvir@hv.se

[1] University West, 46186 Trollhättan, Sweden

Springer

coatings and influence the resultant thermal conductivity of the coating significantly. The heat transfer mechanisms through solid yttria stabilized zirconia (YSZ) and gas in the defects in SPS coatings can be significantly different due to the distinct microstructure of SPS coatings than the conventional coatings and are not fully understood yet. Therefore, fundamental understanding of the individual influence of the features present in the SPS coatings on thermal conductivity is of key importance.

As explained by Golosnoy et al. (Ref 15), the possible contributing modes of heat transfer in 8 wt.% YSZ atmospheric plasma sprayed (APS) TBCs which influence the overall thermal conductivity of the TBC are conduction through the solid YSZ, conduction through the gases in pores, radiative heat transfer and some contribution from convection if segmented cracks are present. At ambient temperature and pressure, in such coatings conductive heat transfer through solid YSZ is largely predominant followed by conduction through the gases in pores. Radiative heat transfer is significant only at higher temperature (greater than 1500 K) (Ref 16). Convection in such coatings can be significant only if the thick and through vertical cracks or segmented cracks are present, which allow the hot gases to pass through them easily and increase the thermal conductivity (Ref 15). Hence, crucial modes which can influence the thermal conductivity at ambient temperature and pressure are conduction through solid YSZ and conduction through gases in pores. For the fully dense, 8 wt.% tetragonal YSZ, the thermal conductivity at ambient conditions is ∼2.5 W/mK (Ref 16). In reality, since the coating is not fully dense and consists of many defects such as crystallite boundaries, pores and cracks, the overall thermal conductivity value is lower than that of the fully dense YSZ, since these defects act as scattering sites for the phonons. This shows that more scattering interfaces are preferred in the form of microstructural defects in TBCs to get lower thermal conductivity.

Conduction through gas in the pores is due to the molecular collisions within the pore. This mode of heat transfer becomes significant in the coating if the pore size is greater than 1 μm and hence can increase the overall thermal conductivity (Ref 16). In general, conventional APS TBCs have pores larger than 1 μm.

Similar to conventional coatings, all heat transfer modes which contribute in influencing the thermal conductivity are also valid for 8 wt.% YSZ SPS TBCs. Presence of fine (submicron or nano-size) microstructural defects enhance the phonon scattering in these coatings which can lower the overall thermal conductivity by conduction through solid YSZ. Also, since the pores present in SPS coatings are in submicron or nano-size range, conductivities in the gas within the pores significantly reduce and can go below that

of free gas (Ref 15, 16). Again, radiation heat transfer can be neglected here as well at ambient conditions.

The main objective of this work was to investigate the individual influence of microstructural defects present in columnar SPS coatings which can influence the final thermal conductivity using experimental and modeling techniques. The modeling technique was used to study the effect of individual microstructural features separately which could provide an indication for optimization of the coating microstructure in order to obtain low thermal conductivity.

Experimental

Sample Production

Five different types of coatings designated as S1, S2, S3, S4 and S5 were produced using the Axial III high-power plasma torch (Northwest Mettech Corp., Vancouver, Canada) and Nanofeed 350 suspension feed system. Ethanol-based suspension of 8 wt.% YSZ of powder size (D_{50}) around 500 nm and solid loading of 25 wt.% was used. A complete TBC system from bottom to top had a first Hastelloy®X substrate with a metallic bond coat of CoNiCrAlY material, AMDRY 9951 (Oerlikon Metco, Wholen, Switzerland) as a middle layer which was deposited using a high velocity air-fuel (HVAF) spray system (Uniquecoat, Richmond, USA); and the top layer was 8 wt.% YSZ ceramic. Nearly the same thickness of around 200 μm bond coat was applied in all types of coatings. Substrates used were square plates (25 mm × 25 mm × 1.6 mm) and buttons (25 mm diameter and 6 mm thickness).

It is relevant to emphasize that the authors' group has been working on TBCs deposited with the above suspension for the past three years (Ref 13, 14), and the purpose of this study was not to conduct an experimental program to understand the spray parameters impact. Instead, it was to understand the role of different microstructural features in reducing the coating thermal conductivity. Hence, based on the previous experience, authors have selected discrete parameters similar to that of reported in previous work (Ref 13, 14) to generate these five columnar structured coatings with different porosity distribution and thermal properties.

All coatings were prepared after spraying for further microstructural characterization. Metallographic sample preparation involved sectioning using diamond cutting blade; mounting the cross sections in a low viscosity epoxy resin using a vacuum impregnation technique; grinding and finally polishing semi automatically using a Buehler PowerPro 5000 (Buehler, USA) machine.

Thermal Conductivity

Measurement for thermal conductivity was indirectly done with the help of laser flash analysis technique. The equation used (Ref 17) to calculate the thermal conductivity was:

$$\left(\lambda = \alpha \cdot C_p \cdot \rho \right)$$

where λ (W/mK) is thermal conductivity of the coating; α (m^2/s) is thermal diffusivity; C_p (J Kg/K) is specific heat capacity of the material and ρ (Kg/m^3) is the density of the coating. Thermal diffusivity was measured using laser flash analysis method. A Netzsch Laser Flash Apparatus LFA 427 system (Netzsch Gerätebau GmbH, Germany) was used to measure the same. Thermal diffusivity was measured both at room temperature in air.

Samples for LFA were prepared by water jet cutting 10 mm round coupon from the 25 mm square plate as a complete TBC system. The measurements were then taken on the samples which were also graphite coated prior to the measurement, due to the relatively transparent nature of YSZ material to the laser used. The detailed description about the LFA experiment was discussed elsewhere (Ref 5).

Column Density

The measurement of column density was done using scanning electron microscope (SEM) micrographs which were then analyzed with an ImageJ public domain free software (Ref 18). Total 35 SEM micrographs were taken for each sample at 300× magnification across the 25 mm sample's cross section. A straight line of fixed length was drawn at half of the coating thickness. All the columnar spacing (vertical spacing between two adjacent columns) intercepting the line in the micrograph was counted as a columnar spacing. The column density was calculated from each micrograph by using:

Column density (vertical cracks/mm)

$$= \frac{\text{Number of columnar spacing/vertical cracks intersecting the line}}{\text{True length of the line}}$$

The final column density was taken as an average of 35 column density measurements.

Porosity Measurement by Water Infiltration Technique

The experimental porosity measurement was carried out with weight difference by the water infiltration method. Ceramic coatings were first removed from the substrates by placing the coating in an aqua regia, a mixture of concentrated HNO_3 and HCl in the ratio (by volume) of 1:3, respectively, the recipe comes originally from GKN aerospace (Trollhättan, Sweden). Around 6-12 h, the samples were then kept in the solution and removed soon after the coatings got separated from the substrate. Over etching of the coating can increase the nano-porosity in the coating; hence, it was made sure that the coating was removed from the solution soon it got separated. Finally, the removed ceramic coating was cleaned by alcohol, dried and weighed. Ceramic coatings were then placed in a beaker containing water and kept in a vacuum for 10 min to force the water into the pores. It was un-vacuumed slowly and vacuumed again for 10 min. This was repeated five times to ensure the proper filling of water inside the pores. All the wet samples were then weighed one by one with the help of an electronic balance. The procedure was repeated on the same sample for three times to get a statistical significance.

The calculation of porosity was then done by using the following mathematical relation:

$$\text{Porosity} = \frac{V_V}{V_T} = \left\{ \frac{\frac{W_{H_2O}}{\rho_{H_2O}}}{\left[\frac{W_{dry}}{\rho_{YSZ}} + \frac{W_{H_2O}}{\rho_{H_2O}} \right]} \right\} \quad \text{where,}$$

$$W_{H_2O} = W_{wet} - W_{dry}$$

Here, V_V, V_T, W_{H_2O}, W_{wet}, W_{dry}, ρ_{YSZ} & ρ_{H_2O} are the volume of voids/pores, total volume, weight of water droplets present in the pores, weight of wet sample, weight of dry sample, density of 8 wt.% YSZ and density of water, respectively. All the parameters were measured in the CGS unit system. Density of water was assumed to be 1 g/cc.

X-ray diffraction

X-ray diffraction (XRD) was used to analyze the different phases present in the coatings and measure the crystallite size or more precisely average sizes of coherently scattering domains which were determined according to the Fundamental Parameters Approach (Ref 13). XRD analysis was carried using a Power D8 Discover diffractometer (Bruker AXS, Germany) with Cu-$K\alpha$ radiation in the 20°-90° 2θ range. Details about the XRD equipment and the experiments can be found in an earlier work (Ref 7).

Modeling

Thermal conductivity of SPS coatings was predicted by using the object-oriented finite element (OOF) method (Ref 19-21). In this method, microscopic images taken by SEM were used to create a finite element mesh for the analysis

work. OOF provides an advantage over other methods since this method can capture the detailed microscopic features such as cracks, pores, different phases etc. Thus, it is suitable for thermal conductivity prediction of TBCs and has been utilized extensively in previous works (Ref 22-28). Detailed explanation about the OOF method can be found in Ref (19, 21). For this study, OOF2 public domain software package (Ref 29) has been used. Complete modeling procedure is described in detail below.

Step 1: Acquiring SEM Images at Two Magnifications

The SPS samples were observed under the SEM in backscattered mode, and images were taken at two different magnification levels, 1000× and 10,000× from each sample, see Fig. 1(a) and (b). These magnification levels were selected in order to capture the two different size scale features that can be seen in all the SPS samples, which were submicron-/nano-level pores and micron-level features like large pores, vertical cracks, columnar spacing etc. At 1000× magnification level, columnar spacing can be seen easily, but not the submicron-/nano-level pores, see Fig. 1(a). So, 10,000× magnification level was selected to capture the submicron-/nano-level pores, see Fig. 1(b). At 10,000×, SEM images were captured from an area away from the columnar spacing so that they contain only small-scale pores. At each magnification level, 20 images were taken all across the coating cross section (25 mm) to represent the coating microstructure. This two magnification technique was successfully used in the literature to analyze SPS TBC microstructures (Ref 28).

Step 2: Binary Image Generation for 10,000× Images

First, 10,000× images were taken into consideration. SEM gray-scale images were converted to binary images with ImageJ (Ref 18) using threshold value technique. Due to the binary conversion, pores in the SEM images were converted to white color and the YSZ material areas were converted to black color, see Fig. 2. The threshold value was selected carefully so that the generated binary image pore distribution closely matches the actual distribution of pores. After the conversion, a finite element mesh was generated in OOF2 as described in step 3.

Step 3: Modeling of 10,000× Images in OOF2

The generated 10,000× binary images were then imported to the OOF2. Two pixel groups were produced in the OOF2, namely YSZ and PORE. Black color pixels in the images were assigned to YSZ material group, and white color pixels were assigned to PORE material group. Thermal conductivity value of 2.5 W/mK (Ref 16) was assigned to the YSZ material groups, and thermal conductivity of atmospheric air, 0.025 W/mK (Ref 16), was assigned as the thermal conductivity for the PORE material group assuming that pores contain air. An adaptive meshing procedure was used to create a finite element mesh based on the image features and colors. Finer elements were generated near the interface boundaries of the PORE and YSZ pixel groups in order to account for higher thermal gradients, see Fig. 3. The smallest size of the elements was selected in such a way that it creates a smooth interface between PORE pixels and the YSZ pixels as in the actual microstructure.
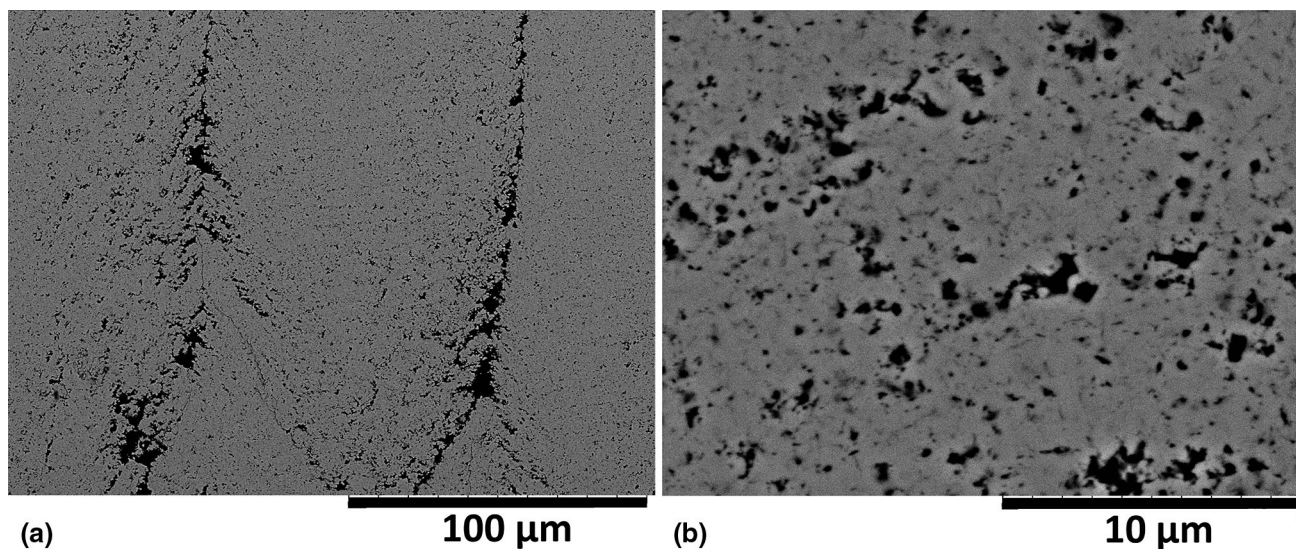

Fig. 1 (a) SEM image of a coating cross section of a sample at (a) 1000× magnification level. (b) 10,000× magnification level
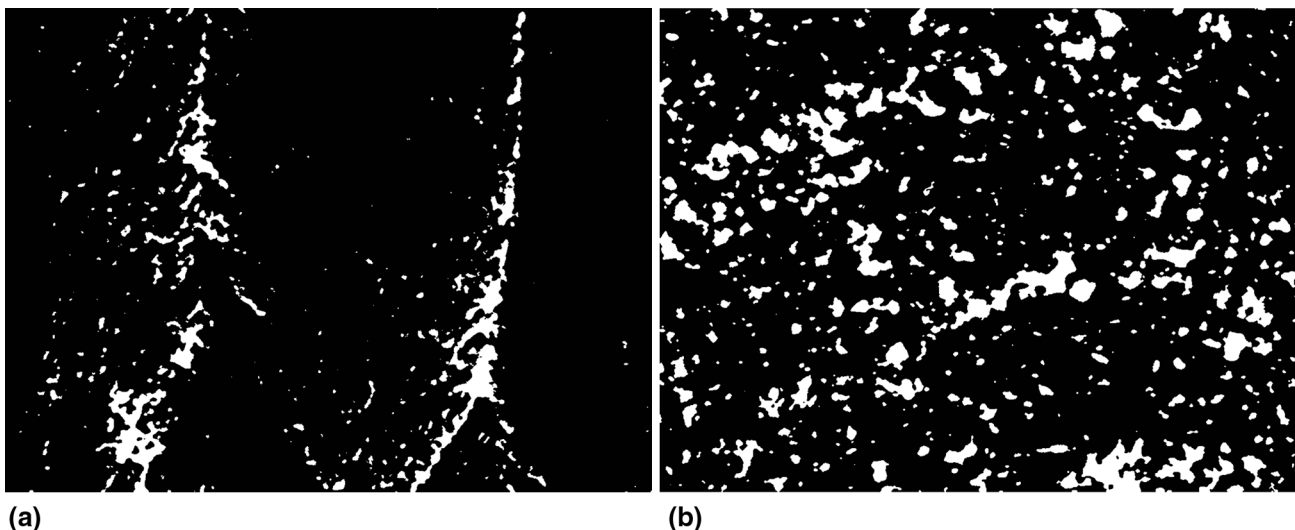
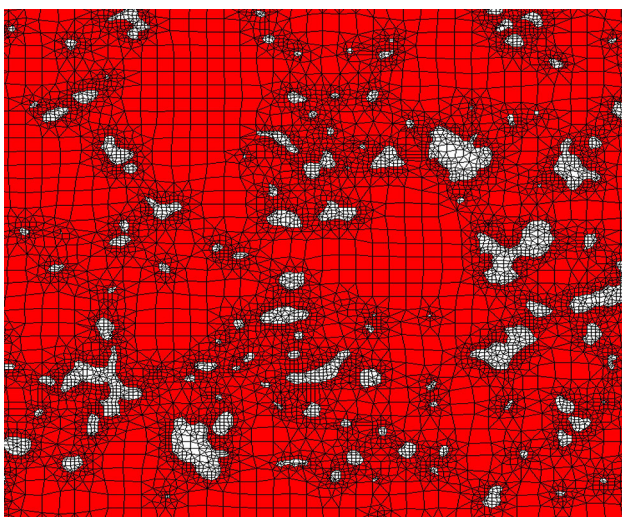**Fig. 2** (a) Binary image after removing the scale bar area of (a) Fig. 1(a). (b) Fig. 1(b)

Fig. 3 Part of the finite element mesh generated in OOF2 (YSZ material area is shown in red color for the visualization purpose)
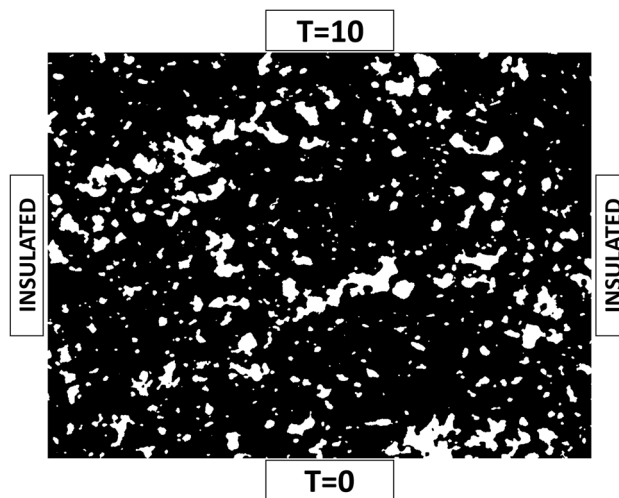

Fig. 4 Boundary conditions applied to the binary image prior to model it in OOF2

Step 4: Binary Image Generation for 1000× Images

The 1000× magnification images were taken into consideration. These images were also converted into binary images as described above using the ImageJ as described in step 2 above, see Fig. 2. After converting the SEM images to binary, it was observed that some small-scale features which can be seen and already considered in 10,000× images also appear in 1000×. Even though their area fraction was considerably lower than the area of large-scale features, these small-scale features were filtered out from the 1000× binary images so that the error due to the repetition of the features in thermal conductivity analysis can be minimized.

Image analysis porosity value was calculated by using the following equation:

Thereafter boundary conditions were applied as shown in Fig. 4. Models were then analyzed, and the heat flux across the cross section was calculated with OOF2. The thermal conductivity value was calculated by solving the Fourier's law of heat conduction which is:

$$\left(\dot{Q} = -\lambda A \frac{\Delta T}{\Delta X} \right).$$

Here $\dot{Q}$ (W) is the heat flux across the cross section, λ (W/mK) is the thermal conductivity of the coating area, A (m^2) is the cross-sectional area parallel to the top and bottom boundaries, ΔT (K) is the temperature gradient, and ΔX (m) is the thickness of the model perpendicular to the coating surface.
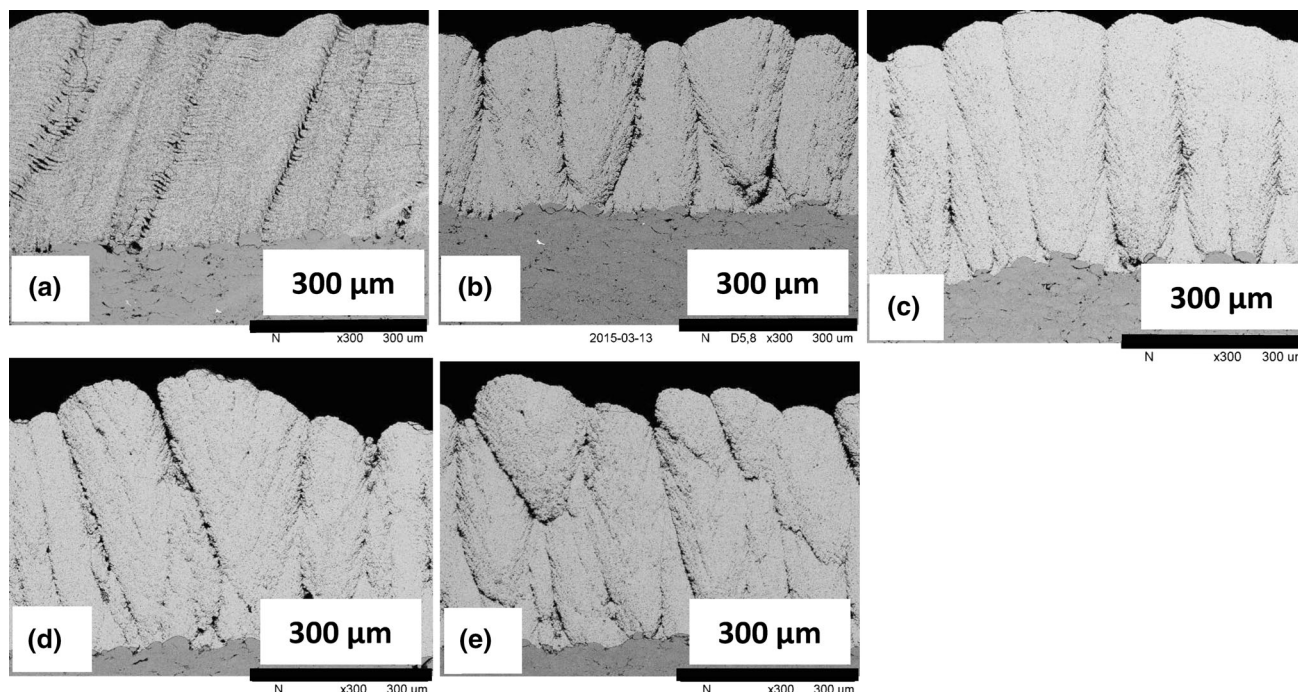
Fig. 5 Cross sections of SPS TBCs showing columnar structure for all five types S1, S2, S3, S4 and S5, respectively, shown in figure (a-e)

$$\text{Image analysis porosity} = \text{Average porosity at } 10,000 + \text{Average porosity at } 1000\times$$

$$(\text{Eq 1})$$

Step 5: Modeling of 1000× Images in OOF2

1000× binary images were then imported into the OOF2. The calculated thermal conductivity at 10,000× was used as the YSZ thermal conductivity instead of bulk YSZ as the fine-scale porosity was not considered in the 1000× images. PORE conductivity was kept unchanged. Same boundary conditions were given as described in step 3, and the model was analyzed in OOF2. Thereafter, the overall thermal conductivity was calculated using the heat conduction equation as described earlier, and it was taken as the thermal conductivity of the coating.

Following major assumptions were made for the calculation.

1. Heat transfer through the coating thickness happens only by means of conduction. The convection and radiation heat transfer is negligible.
2. Heat transfer only happens through the coating thickness direction. Transverse heat transfer in the coating can be neglected due to significantly larger dimensions in transverse directions.
3. Knudsen effect (Ref 30) was not taken into account when considering the thermal conductivity of air inside the pores.

Results and Discussions

Microstructure

Figure 5 shows the cross section of all the coatings and also a simplified schematic of a columnar structure highlighting the important defects in the microstructure. It can be observed from Fig. 5 that all coatings have shown a columnar structure. The important thing to be noted here is that there were no fine cracks unlike conventional APS coatings were observed in these columnar SPS coatings. This was confirmed by looking at higher magnifications for all coatings in SEM, see Fig. 1(b).

Important defects in TBCs which can influence the thermal conductivity of the coating are porosity at a larger scale and crystallite boundaries at a smaller scale (Ref 29, 30). These defects act as a barrier to the heat flow which lowers the thermal conductivity of the coating. In conventional APS coatings, the important microstructural defects are delamination, globular pores, fine cracks and fine-scaled porosity (in the micron range) (Ref 29). Unlike conventional APS coatings, porosity in these coatings includes micron, submicron or nano-pores within the columns and vertical cracks or columnar spacing between the columns (see Fig. 1 at 1000× and 10,000×). Distribution of this varied scaled porosity in SPS columnar coatings hence becomes an important issue when it comes to analyzing the thermal conductivity in such coatings.
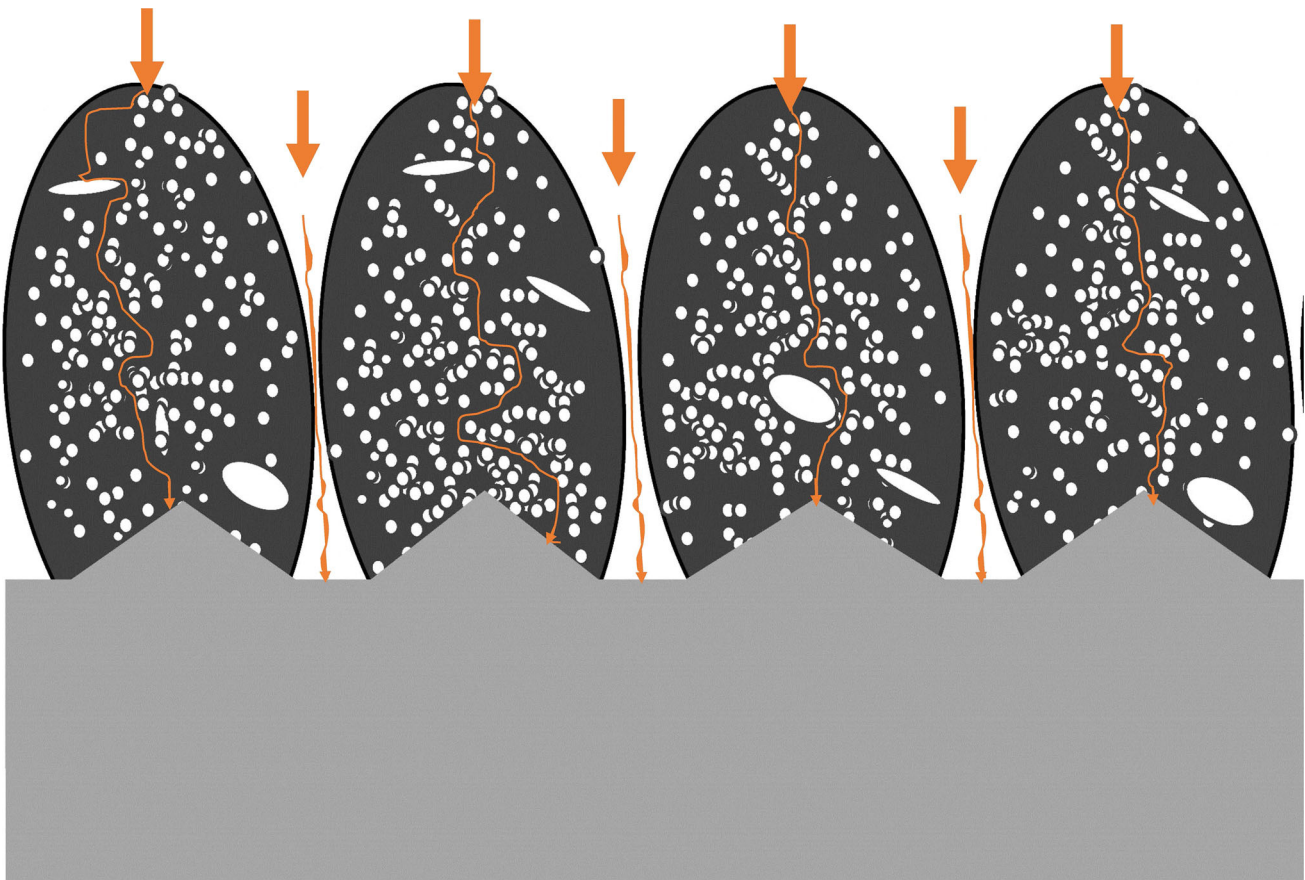
Fig. 6 Simplified schematic of a cross section for columnar structure in SPS TBC showing fine features (micro- and nano-scale pores) and coarse features (columnar spacing/vertical cracks and other large-scaled pores), which play significant role in deciding the overall thermal conductivity of the coating. Also showing the schematic of the heat flow between the columns and within the columns

Simplified schematic shown in Fig. 6 shows the important microstructural features in a columnar structured coating. These features are columnar spacing (a spacing between two adjacent columns separating each other), small- and large-scaled pores within the column. Also, crystallite boundaries which are considered to be an important microstructural defect are not visible at such low magnification and hence not shown in the schematic. Figure 6 helps in understanding the role of different scaled porosity in columnar structured coatings while decreasing the thermal conductivity. It can be seen from the schematic shown that the possible paths for heat flow through these columnar structures are firstly in between the columns (through the spacing) and secondly within the columns. In addition, it can be observed from the schematic that there are significant smaller and larger pores within the columns. These pores can enhance the scattering of phonons and disturb the heat flow within the columns and hence help in reducing the overall coating thermal conductivity. However, inter-columnar spacing can allow easier paths for the heat flow during service conditions due to pressure difference and hence can increase overall coating thermal conductivity.

Phase Analysis and Crystallite Size

Phase analysis using XRD revealed that all the coatings showed mainly tetragonal phase. It should be noted that tetragonal (t') is the desired phase in YSZ material due to its metastable nature nearly up to 1200 °C (Ref 31). Table 1 shows the experimental data measured for all coatings. It can be seen from Table 1 that the crystallite size for S2 was the highest and S1 the lowest, followed by S3, S4 and S5 which showed similar crystallite size among them.

Experimental Porosity and Thermal Conductivity

Table 1 shows the experimental data measured for all coatings. Comparing overall experimental porosity of all five coatings S1, S2, S3, S4 and S5, it can be seen that S1 showed highest (25.2%) followed by S2 (22.7%), whereas

Table 1 Experimentally measured characteristics of the of the samples

Sample designation	S1	S2	S3	S4	S5
Thickness (μm)	388 ± 21	326 ± 22	398 ± 15	416 ± 21	423 ± 28
Column density (crack/mm)	9.8 ± 2.3	11.6 ± 2.0	9.1 ± 2.7	11.3 ± 2.6	13.0 ± 2.8
Experimental porosity (vol.%)	25.2 ± 1.5	22.1 ± 0.5	15.7 ± 2.3	15.8 ± 1.1	14.3 ± 1.9
Crystallite size (nm)	100 ± 1	128 ± 3	116 ± 3	123 ± 3	122 ± 3
Experimental thermal conductivity (W/mK)	0.97	1.1	1.32	1.43	1.53
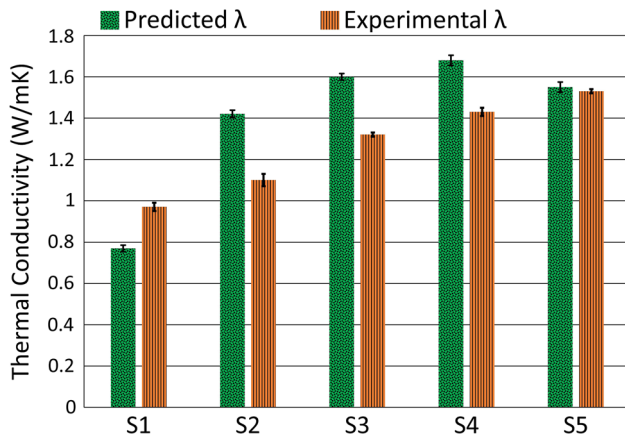
Fig. 7 Experimentally measured and modeling predicted thermal conductivity results
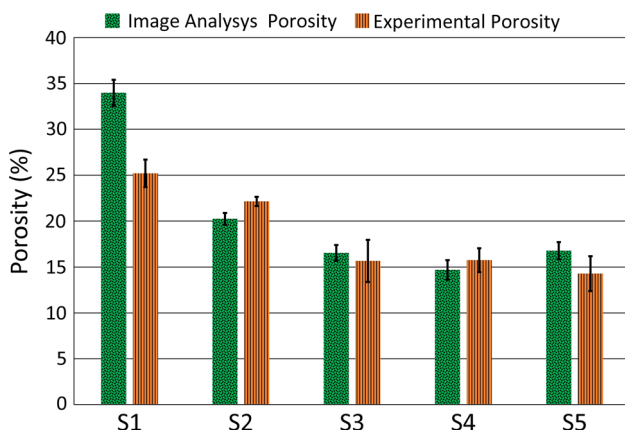
Fig. 8 Porosity results by image analysis and experimental water impregnation technique

S5 showed lowest (14.2%) porosity. Coatings S3 and S4, on the other hand, showed similar porosity around (15.5%) which was lower than S1 and S2 but higher than S5. Also, comparing the column density among these coatings, S5 showed the highest (13.0 cracks/mm), whereas S1 and S3 to be lowest (9.8 and 9.1 cracks/mm respectively); however, coatings S2 and S4 showed 11.6 and 11.3 cracks/mm, respectively.

It can be seen that coating S1 has the lowest thermal conductivity among all five coatings when comparing the

experimental thermal conductivity results. The reasons for the low thermal conductivity can be highest overall porosity and smallest crystallite size among all coatings which means higher number of crystallite boundaries compare to all other coatings. Apart from this, S1 has also showed lower column density relative to other coatings. As explained earlier in "Introduction" and "Microstructure" sections that the presence of higher crystallite boundaries, higher small-scaled pores and lower column density help in reducing the overall thermal conductivity of the coating. This then explains the lowest thermal conductivity of the coating S1. On the other hand, coating S5 showed the highest thermal conductivity. Again, it can be seen that S5 has lowest porosity, large crystallite size and highest column density which explain the higher thermal conductivity in coating S5.

The effect of column density on thermal conductivity is, however, still not fully understood as concluded from a previous detailed characterization work done by the author (Ref 14). Moreover, the effect of enhanced heat flow in inter-columnar spacing is not considered in experimental measurements due to the absence of the pressure difference usually present in TBC service conditions. This would mean that thermal conductivity of these coatings measured experimentally at laboratory scale would be a bit higher than measured values in actual service conditions.

Modeling of Thermal Conductivity

The predicted thermal conductivity values are shown in Fig. 7 with their experimental thermal conductivity values. Out of the five samples, four showed the same trend as the measured value for thermal conductivity. This indicates that the method that has been used for this thermal conductivity prediction is capable enough to catch the different microstructural features and rank the coatings according to their thermal conductivity value.

Except the sample S1, in all the other samples, the predicted thermal conductivity value was above the experimental value, see Fig. 7. There are few reasons that could explain the over prediction of the thermal conductivity. In reality, the coating has many features that can affect the thermal conductivity such as pores, cracks and inter-splat boundaries (Ref 16). These features can help to

reduce the thermal conductivity, but it was difficult to catch all these features due to the limitation in the selected SEM resolution. Higher-resolution SEM images could result in a more accurate analysis. Another reason can be the limitation of 2D geometry of the model. In modeling, the SEM images that were used to predict the thermal conductivity represent only a small fraction of the cross section. So it may not always accurately represent the entire TBC microstructure. Furthermore, 2D images may not exactly represent the 3D microstructure of the TBC. This creates a difference between the predicted and the experimental thermal conductivity. Also, since the Knudsen effect was not taken into account, it may also affect the over prediction of the thermal conductivity.

In sample S1, the predicted thermal conductivity value was less than the experimental value. This can be due to the high porosity level in this coating. The image analysis porosity value was 35% higher than the experimental porosity value, see Fig. 8. SEM images of the coating S1 showed many closed pores compared to SEM images of a sample S2 which had the experimental porosity value close to S1, see Fig. 9. Also, this coating did not show clear columnar crack-like features, see Fig. 10. Larger closed pores may result in lower experimental porosity values since these pores may not be accessible by water in the water impregnation technique. This effect would result in higher experimental density values than reality. From Eq 1, it can be concluded that experimental thermal conductivity
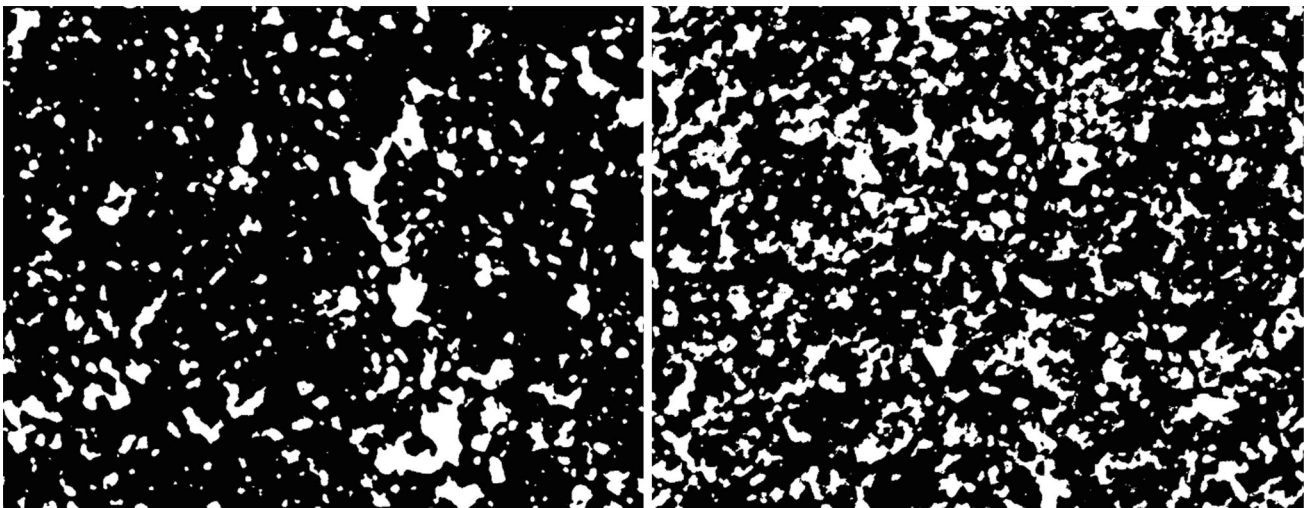

Fig. 9 Binary image of coating S1 (right) and coating S2 (left) showing the comparison of close porosity content at 10,000×
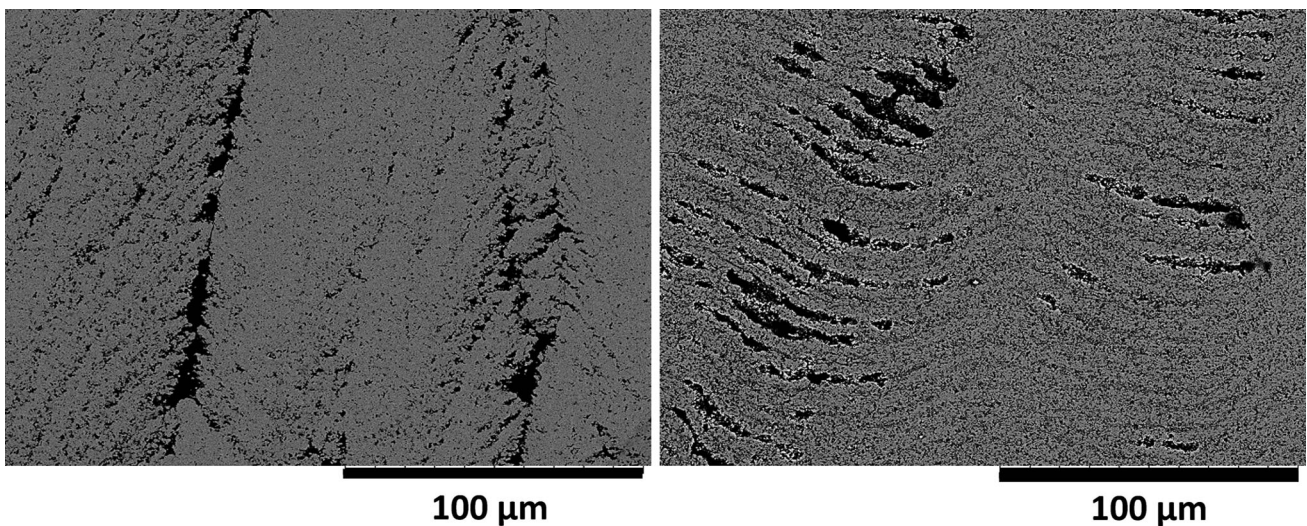

Fig. 10 SEM image of coating S1 at 1000× (right) which does not show clear columnar crack-like features as compared to coating S2 (left)

value will then be higher than reality due to the higher experimental density. This could be a reason for the predicted thermal conductivity value to be less than the experimental value for coating S1. Similarly, in coating S5, the image analysis porosity value was 17% higher than the experimental value, thus indicating that coating S5 also contains closed pores but not as much as in coating S1. Therefore, the experimental value and the predicted value are almost same.

Despite the drawbacks of the modeling analysis, thermal conductivity showed good correlation with total porosity, see Fig. 11. Kassner et al. (Ref 32) also have shown that a good correlation exits in thermal conductivity and porosity in SPS coatings. This indicates that the thermal conductivity of the SPS coatings can be significantly influenced by the total porosity level in the coating. Thus, tailoring the porosity in coatings will be a key factor to tailor the thermal conductivity value of SPS TBC coatings.

Effect of Individual Microstructural Features

The individual effect of the two scale features present in the coating microstructure which are fine (micro- and nano-
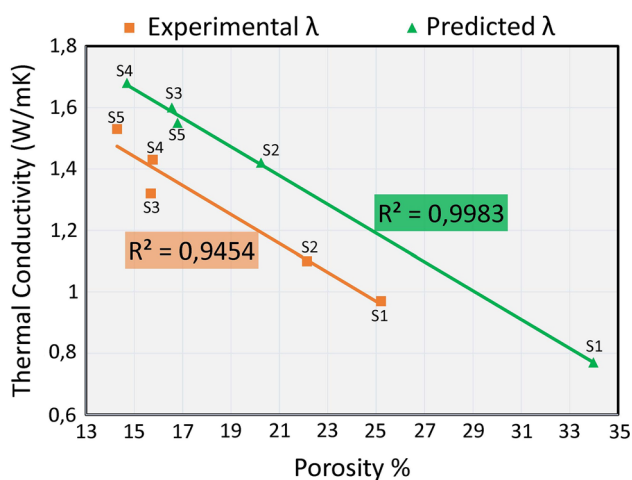
pores) and coarse (columnar spacing/vertical cracks and other large pores) features was studied separately. Table 2 shows the percentage thermal conductivity value reduction (from the bulk material conductivity value) due to its different porosity features present at two different magnification levels. At 10,000×, mainly the fine (micro- and nano-scale pore) features are visible and hence can be responsible for reducing the thermal conductivity, whereas at 1000× it can be due to the coarse (columnar spacing/vertical cracks and other large-scale pores) features. It can be clearly seen that the fine-scale porosity has a higher impact on reducing the thermal conductivity than the coarse features in the coating. One could argue that this is due to the higher porosity values at that level. Therefore, ratio between thermal conductivity reduction and the porosity level at the relevant magnification can help to compare the effect of the features without having to consider the individual porosity level.

It can be noticed that, in all the samples, this ratio at 10,000× was higher than at 1000×. This higher ratio at 10,000× could be due to the effect of even porosity distribution at this magnification compare to the isolated coarse features at 1000×. Therefore, fine features have a higher impact in reducing the thermal conductivity. It is clear from these results that having an evenly distributed fine-scale features can be beneficial for reducing the thermal conductivity of the SPS TBCs than having isolated coarse features.

Effect of Convective Heat Transfer

Effect of inter-columnar spacing/vertical cracks on thermal conductivity due to convection was also verified using this model in a simplified way. S3 coating which showed the least vertical crack density was considered for this. In the final step of the modeling procedure, where the columnar spacing and other large features were considered (see Fig. 2a), heat transfer due to convection through such cracks was simulated by using a thermal conductivity of air 10 times higher (0.25 W/mK) than the value used in step 3.

Fig. 11 Correlation between porosity and the thermal conductivity

Table 2 Modelled percentage thermal conductivity reduction at the two different magnification levels

Sample	Porosity at 10,000× (in %)	Porosity at 1000× (in %)	λ reduction at 10,000× (in %)	λ reduction at 1000× (in %)	Total λ reduction (in %)	Ratio between % λ reduction and porosity % at 10,000×	Ratio between % λ reduction porosity % at 1000×
S1	26.75	7.23	60.8	8.4	69.20	2.3	1.2
S2	12.86	7.38	30.8	12.4	43.20	2.4	1.7
S3	12.27	4.28	28.8	7.2	36.00	2.3	1.7
S4	10.30	4.40	24.8	8	32.80	2.4	1.8
S5	11.47	5.32	27.2	10.8	38.00	2.4	2.0

Table 3 Change in S3 coating λ with air conductivity in vertical cracks/columnar spacing

Thermal conductivity of air used in modeling step 5 (W/mK)	0.025	0.25
Resultant coating λ (W/mK)	1.60	1.66

The calculated final thermal conductivity value for the S3 coating (Refer Table 3) was increased by an amount of 1.04 times only, indicating that the heat transfer in the inter-columnar spacing/vertical cracks by means of convection does not have a significant effect on the overall thermal conductivity of the coating.

These results show that the modeling technique used in this work is capable of capturing the microstructural features and predict the thermal conductivity of the coatings in a reasonable way. Additionally, modeling is a more effective technique than experiments when comparing and ranking thermal conductivity of different coatings as it effectively captures the effect of closed pores on density and thermal conductivity.

Summary and Conclusions

In this study, five SPS TBC samples' thermal conductivity values were analyzed by using both modeling with OOF2 and standard experimental techniques. Two different magnification-level SEM images were used for the modeling work. The experimental thermal conductivity values were calculated by using LFA. The modeling method developed in this study was able to predict and rank the SPS coatings' thermal conductivity values efficiently. This method was also able to capture the effect of closed pores on thermal conductivity, which was not included in the experimental method due to the limitation in the measurement of density using the water impregnation technique. The results of this work show that OOF seems to be a powerful tool to predict and rank thermal conductivity of SPS TBCs. In addition, experimental results showed that higher porosity and lower crystallite size can result in lower thermal conductivity. The individual influence of fine features (micro- and nano-pores) and coarse features (vertical cracks/columnar spacing) was studied by modeling and it was found that the presence of evenly distributed fine features can have significant effect in reducing the thermal conductivity compared to the coarse features.

References

1. R.A. Miller, Thermal Barrier Coatings for Aircraft Engines: History and Directions, *J. Therm. Spray Technol.*, 1997, **6**(1), p 35-42
2. N. Curry, Z. Tang, N. Markocsan, and P. Nylén, Influence of Bond Coat Surface Roughness on the Structure of Axial Suspension Plasma Spray Thermal Barrier Coatings—Thermal and Lifetime Performance, *Surf. Coat. Technol.*, 2015, **268**, p 15-23
3. K. VanEvery, M.J.M. Krane, R.W. Trice, H. Wang, W. Porter, M. Besser, D. Sordelet, J. Ilavsky, and J. Almer, Column Formation in Suspension Plasma-Sprayed Coatings and Resultant Thermal Properties, *J. Therm. Spray Technol.*, 2011, **20**(4), p 817-828
4. U. Schulz, C. Leyens, K. Fritscher, M. Peters, B. Saruhan-Brings, O. Lavigne, J.-M. Dorvaux, M. Poulain, R. Mévrel, and M. Caliez, Some Recent Trends in Research and Technology of Advanced Thermal Barrier Coatings, *Aerosp. Sci. Technol.*, 2003, **7**(1), p 73-80
5. A. Ganvir, N. Curry, N. Markocsan, P. Nylén, and F.-L. Toma, Comparative Study of Suspension Plasma Sprayed and Suspension High Velocity Oxy-Fuel Sprayed YSZ Thermal Barrier Coatings, *Surf. Coat. Technol.*, 2015, **268**, p 70-76
6. A. Ganvir, N. Curry, S. Govindarajan, and N. Markocsan, Characterization of Thermal Barrier Coatings Produced by Various Thermal Spray Techniques Using Solid Powder, Suspension, and Solution Precursor Feedstock Material, *Int. J. Appl. Ceram. Technol.*, 2015, p n/a-n/a
7. H. Kassner, R. Siegert, D. Hathiramani, R. Vassen, and D. Stover, Application of Suspension Plasma Spraying (SPS) for Manufacture of Ceramic Coatings, *J. Therm. Spray Technol.*, 2008, **17**(1), p 115-123
8. T.R. Kakuda, A.M. Limarga, T.D. Bennett, and D.R. Clarke, Evolution of Thermal Properties of EB-PVD 7YSZ Thermal Barrier Coatings with Thermal Cycling, *Acta Mater.*, 2009, **57**(8), p 2583-2591
9. J.R. Nicholls, K.J. Lawson, A. Johnstone, and D.S. Rickerby, Methods to Reduce the Thermal Conductivity of EB-PVD TBCs, *Surf. Coat. Technol.*, 2002, **151-152**, p 383-391
10. K. Matsumoto, Y. Itoh, and T. Kameda, EB-PVD Process and Thermal Properties of Hafnia-Based Thermal Barrier Coating, *Sci. Technol. Adv. Mater.*, 2003, **4**(2), p 153
11. A.F. Renteria, B. Saruhan, U. Schulz, H.-J. Raetzer-Scheibe, J. Haug, and A. Wiedenmann, Effect of Morphology on Thermal Conductivity of EB-PVD PYSZ TBCs, *Surf. Coat. Technol.*, 2006, **201**(6), p 2611-2620
12. A. Ganvir, N. Curry, N. Markocsan, P. Nylen, M. Vilemova, and Z. Pala, Influence of Microstructure on Thermal Properties of Columnar Axial Suspension Plasma Sprayed Thermal Barrier Coatings. In *Thermal Spray 2015: Proceedings from the International Thermal Spray Conference (May 11-14, 2015, Long Beach, California, USA)*, Long Beach, California, 2015, p 498-505
13. A. Ganvir, N. Curry, S. Björklund, N. Markocsan, and P. Nylén, Characterization of Microstructure and Thermal Properties of YSZ Coatings Obtained by Axial Suspension Plasma Spraying (ASPS), *J. Therm. Spray Technol.*, 2015, p 1-10.
14. A. Ganvir, N. Curry, N. Markocsan, P. Nylén, S. Joshi, M. Vilemova, and Z. Pala, Influence of Microstructure on Thermal Properties of Axial Suspension Plasma-Sprayed YSZ Thermal Barrier Coatings, *J. Therm. Spray Technol.*, 2015, **25**(1-2), p 202-212
15. I.O. Golosnoy, S.A. Tsipas, and T.W. Clyne, An Analytical Model for Simulation of Heat Flow in Plasma-Sprayed Thermal Barrier Coatings, *J. Therm. Spray Technol.*, 2005, **14**(2), p 205-214

16. I.O. Golosnoy, A. Cipitria, and T.W. Clyne, Heat Transfer Through Plasma-Sprayed Thermal Barrier Coatings in Gas Turbines: A Review of Recent Work, *J. Therm. Spray Technol.*, 2009, **18**(5-6), p 809-821

17. R. Taylor, Thermal Conductivity Determinations of Thermal Barrier Coatings, *Mater. Sci. Eng., A*, 1998, **245**(2), p 160-167

18. ImageJ Software, *Image Processing and Analysis in Java*. http://imagej.nih.gov/ij/. Accessed 17 Nov 2014.

19. S.A. Langer, E.R.F. Jr., and W.C. Carter, OOF: Image-Based Finite-Element Analysis of Material Microstructures, *Comput. Sci. Eng.*, 2001, **3**(3), p 15-23

20. P. Michlik and C. Berndt, Image-Based Extended Finite Element Modeling of Thermal Barrier Coatings, *Surf. Coat. Technol.*, 2006, **201**(6), p 2369-2380

21. A.C.E. Reid, S.A. Langer, R.C. Lua, V.R. Coffman, S.-I. Haan, and R.E. García, Image-Based Finite Element Mesh Construction for Material Microstructures, *Comput. Mater. Sci.*, 2008, **43**(4), p 989-999

22. J.P. Angle, Z. Wang, C. Dames, and M.L. Mecartney, Comparison of Two-Phase Thermal Conductivity Models with Experiments on Dilute Ceramic Composites, *J. Am. Ceram. Soc.*, 2013, **96**(9), p 2935-2942

23. M. Gupta and P. Nylén, Design of Low Thermal Conductivity Thermal Barrier Coatings by Finite Element Modelling, presented at the SMT24, Dresden, September 7-9, 2010, 2011, p 353-365.

24. M. Gupta and P. Nylén, Structure-property Relationships in Thermal Barrier Coatings by Finite Element Modelling, presented at the Twenty Fifth International Conference on Surface Modification Technologies, 2012, p 175-184.

25. A.D. Jadhav, N.P. Padture, E.H. Jordan, M. Gell, P. Miranzo, and E.R. Fuller, Jr., Low-Thermal-Conductivity Plasma-Sprayed Thermal Barrier Coatings with Engineered Microstructures, *Acta Mater.*, 2006, **54**(12), p 3343-3349

26. Z. Wang, A. Kulkarni, S. Deshpande, T. Nakamura, and H. Herman, Effects of Pores and Interfaces on Effective Properties of Plasma Sprayed Zirconia Coatings, *Acta Mater.*, 2003, **51**(18), p 5319-5334

27. M. Gupta, P. Nylén, and J. Wigren, A Modelling Approach to Designing Microstructures in Thermal Barrier Coatings, *J. Ceram. Sci. Technol.*, 2013, **4**(2), p 85-92

28. M. Gupta, N. Curry, P. Nylén, N. Markocsan, and R. Vaßen, Design of Next Generation Thermal Barrier Coatings—Experiments and Modelling, *Surf. Coat. Technol.*, 2013, **220**, p 20-26

29. OOF: Finite Element Analysis of Microstructures. *OOF: Finite Element Analysis of Microstructures*: http://www.ctcms.nist.gov/oof/oof2/. Accessed: 17 Nov 2014.

30. J.H. Qiao, R. Bolot, H.L. Liao, and C. Coddet, Knudsen Effect on the Estimation of the Effective Thermal Conductivity of Thermal Barrier Coatings, *J. Therm. Spray Technol.*, 2013, **22**(2-3), p 175-182

31. R. A. Miller, J. L. Smialek, and R. G. Garlick, Phase Stability in Plasma-Sprayed, Partially Stabilized Zirconia-Yttria. In *Science and Technology of Zirconia, Advances in Ceramics*, vol. 3, Westerville, OH: The American Ceramic Society, 1981, p 241-253

32. H. Kassner, A. Stuke, M. Rodig, R. Vassen, and D. Stover, "Influence of Porosity on Thermal Conductivity and Sintering in Suspension Plasma Sprayed Thermal Barrier Coatings, *Adv. Ceram. Coat. Interfaces III, Ceram. Eng. Sci. Proc.*, 2009, **46**, p 147